



This is a repository copy of *A high-power factor Vernier machine with coil pitch of two slot pitches*.

White Rose Research Online URL for this paper:  
<http://eprints.whiterose.ac.uk/139342/>

Version: Accepted Version

---

**Article:**

Liu, Y., Li, H.Y. and Zhu, Z.Q. [orcid.org/0000-0001-7175-3307](https://orcid.org/0000-0001-7175-3307) (2018) A high-power factor Vernier machine with coil pitch of two slot pitches. *IEEE Transactions on Magnetics*, 54 (11). 8105405. ISSN 0018-9464

<https://doi.org/10.1109/TMAG.2018.2839976>

---

© 2018 IEEE. Personal use of this material is permitted. Permission from IEEE must be obtained for all other users, including reprinting/ republishing this material for advertising or promotional purposes, creating new collective works for resale or redistribution to servers or lists, or reuse of any copyrighted components of this work in other works. Reproduced in accordance with the publisher's self-archiving policy.

**Reuse**

Items deposited in White Rose Research Online are protected by copyright, with all rights reserved unless indicated otherwise. They may be downloaded and/or printed for private study, or other acts as permitted by national copyright laws. The publisher or other rights holders may allow further reproduction and re-use of the full text version. This is indicated by the licence information on the White Rose Research Online record for the item.

**Takedown**

If you consider content in White Rose Research Online to be in breach of UK law, please notify us by emailing [eprints@whiterose.ac.uk](mailto:eprints@whiterose.ac.uk) including the URL of the record and the reason for the withdrawal request.



[eprints@whiterose.ac.uk](mailto:eprints@whiterose.ac.uk)  
<https://eprints.whiterose.ac.uk/>

# A High Power Factor Vernier Machine with Coil-Pitch of Two Slot Pitches

Yue Liu, H.Y. Li, and Z.Q. Zhu, *Fellow, IEEE*

Department of Electronic and Electrical Engineering, University of Sheffield, S10 2TN, UK

In this paper, an 18-slot/26-pole Vernier permanent magnet synchronous machine (VPMSM) with coil-pitch of two slot pitches is proposed based on a 9-slot/18-flux-modulation-pole/26-pole VPMSM with concentrated tooth-coil windings. Compared with the original VPMSM, the number of slots is doubled and the phase winding connection is adjusted to reduce the space harmonic content, the phase inductance, and hence, improve the power factor. The study shows that the proposed VPMSM increases power factor from 0.73 to 0.95 with better torque and flux weakening capability. Moreover, a series of VPMSMs with high power factor are proposed from the same design principle and given design guidelines.

**Index Terms**—Concentrated winding, permanent magnet, power factor, Vernier machine.

## I. INTRODUCTION

Vernier permanent magnet synchronous machine (VPMSM) has become a promising candidate in direct drive application because of high torque density and low torque ripple [1] [2]. Quantitative comparisons have been made between VPMSM, conventional PM machines [3] [4] and magnetically-gearred machines [5], showing that the VPMSM has the highest torque density.

However, Vernier machines suffer from lower power factors compared with the traditional PMSMs. Low power factor means power converters of larger sizes are required for the same output power, which increases the cost and hinders the application of the VPMSMs. The low power factor of VPMSM is mainly caused by the increased number of rotor PM poles which leads to a much greater inductive reactance [6]. There are some papers trying to improve the power factor of VPMSMs by using Halbach PM rotor [3] or dual-rotor structure [8] [9]. However, special techniques or complicated structures are needed, hindering their application to common VPMSM designs. Some machine candidates with coil pitch of two slot pitches in [10] and [11] are claimed to have high power factors. Although the structure is simpler, the theoretical basis for the power factor improvement is not investigated, and therefore, no guidelines are proposed on how to design a high power factor VPMSMs by a proper selection of slot/pole combination and winding arrangement. In this paper, an 18-slot/26-pole VPMSM with coil-pitch of two slot pitches is evolved and proposed based on a 9-slot/18-flux-modulation-pole (FMP)/26-pole VPMSM with concentrated tooth-coil windings. Compared with the original machine, the slot number is doubled and the phase winding connection is adjusted in the proposed one to reduce the space harmonic content. The study shows that such design can effectively decrease the phase inductance and improve the power factor with better torque and flux weakening capability. Moreover, a design guideline on slot/pole number selection and winding

arrangement will be provided, a series of high power factor VPMSMs will emerge from the same theoretical basis and design principle.

## II. MACHINE STRUCTURE AND WORKING PRINCIPLE

### A. Power factor of VPMSMs

It has been mentioned in various literatures that VPMSM has a low power factor which hinders its application when considering the optimum combination between the machine and converter. The low power factor of VPMSMs can be explained by the phasor diagram shown in Fig. 1. When a PMSM is under  $I_d=0$  control and the resistance of the stator windings is ignored, the phasors of q-axis current  $I_q$  and the no-load back EMF  $E_0$  are in the same direction, the voltage phasor produced by  $I_q$  and the inductive reactance  $X_q$  has a 90-electrical-degree shift from  $E_0$ , and  $U_0$  is the resultant phasor of terminal voltage. In this case, the power factor can be expressed as:

$$\cos \varphi = \frac{1}{\sqrt{1 + \left(\frac{I_q X_q}{E_0}\right)^2}} \quad (1)$$

$$X_q = \omega L_q = \frac{2\pi}{60} n p_r L_q \quad (2)$$

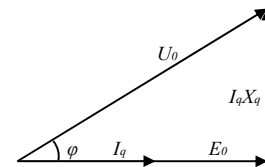


Fig. 1. Phasor diagram.

For a conventional PMSM, there always exists a Vernier counterpart with the same slot number, winding configuration but an increased PM pole number. When compare a conventional PMSM with its Vernier counterpart, the q-axis inductance  $L_q$  of both machines are similar since they share the same winding configuration. However, it can be seen in (2) that the increase in  $X_q$  is proportional to the increase of PM pole number  $p_r$  and is larger than the increase in  $E_0$ . This consequently causes a larger  $\varphi$  and smaller power factor for

VPMSMs. Hence, it can be concluded that the low power factor is an inherent problem for VPMSMs as a result of higher PM pole number. From (2), since  $p_r$  cannot be changed for an existing VPMSM, one of the possible way to reduce  $X_q$  is to reduce the inductance.

*B. Machine Topology Evolution and Principle*

A 9-slot/18-FMP/26-pole VPMSM with concentrated windings is shown in Fig. 2 (a). This is a typical VPMSM with concentrated tooth-coil windings [12] since it satisfies  $p_r=N_f-p_s$ , where  $N_f$  is the number of FMPs in the stator and  $p_s$  is pole pair number of the armature reaction magnetic motive force (MMF). Its armature reaction MMF and spectrum are shown in Fig. 3. It shows that there are abundant harmonics in the MMF waveform. The orders of the main harmonics are 4<sup>th</sup>, 5<sup>th</sup>, 13<sup>th</sup> and 14<sup>th</sup>. It is noteworthy that the main harmonics appear in pairs and with the order difference of 1.

To reduce the inductance of the 9-slot/18-FMP/26-pole VPMSM, the MMF harmonics need to be reduced. With this aim, an 18-slot/26-pole VPMSM with coil-pitch of two slot pitches is proposed. The proposed machine is evolved from the original machine via the following steps: (1) Double the number of slots so that in the proposed machine the number of stator slots  $N_s$  equals to  $N_f$  in the original machine, as shown in Fig. 2 (b). (2) Divide the windings of phase (A, B, C) in Fig 2 (b) into two groups denoted as (A1, B1, C1) and (A2, B2, C2). (3) In the proposed machine, configure (A1, B1, C1) in the same way with (A, B, C), with the coil spanning two slot pitches. (4) In the proposed machine, configure (A2, B2, C2) with a 180-mechanical-degree shift from (A1, B1, C1) (5) Invert the polarity of (A2, B2, C2).

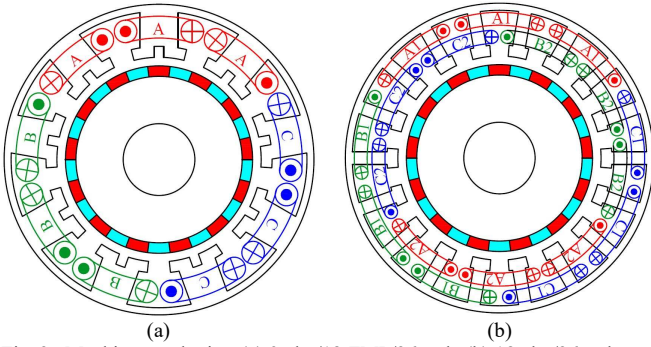


Fig. 2. Machine topologies. (a) 9-slot/18-FMP/26-pole (b) 18-slot/26-pole

By doing this, the armature reaction MMF space harmonics of even orders can be effectively eliminated without affecting the harmonics of odd orders. Take the 4<sup>th</sup> and 5<sup>th</sup> harmonics for example as shown in Fig. 4, the 4<sup>th</sup> harmonics generated by phase A1B1CA and A2B2C2 have the same phase after a 180-mechanical-degree shift and cancel with each other after the polarity of Phase A2B2C2 is inverted. On the contrary, the 5<sup>th</sup> harmonics generated by phase A1B1CA and A2B2C2 have the opposite phase after a 180-mechanical-degree shift and after Phase A2B2C2 swaps its polarity, they are in phase. Their accumulated waveform is the same with that of the 9-slot/18-FMP/26-pole machine under the same electrical loading. This principle applies not only for the 4<sup>th</sup> and 5<sup>th</sup> harmonics but all the even and odd order harmonics in this

machine. Fig. 3 also shows the armature reaction MMF waveforms generated by phase A1B1C1, A2B2C2 and their accumulated results. It can be clearly seen from its spectrum that all the even order harmonics have been eliminated. For machines with surface PMs, the q-axis inductance  $L_q$  can be calculated by:

$$L_q = \frac{\mu_0 r_g l_{ef}}{g} \int_0^{2\pi} f(\theta) N_a(\theta) d\theta \quad (3)$$

where  $\mu_0$  is the permeability of air,  $r_g$  is the air gap radius,  $g$  is the effective airgap length,  $l_{ef}$  is the effective axial length,  $f(\theta)$  is the 3-phase resultant MMF and  $N(\theta)$  is the winding function [13]. It can be calculated from (3) that  $L_q$  of the 18-slot/26-pole machine is only 42% of the 9-slot/18-FMP/26-pole machine under the same geometry features and number of turns per phase. This proves that reduction of armature reaction space harmonic content can directly reduce the phase inductance, and consequently, improve the power factor.

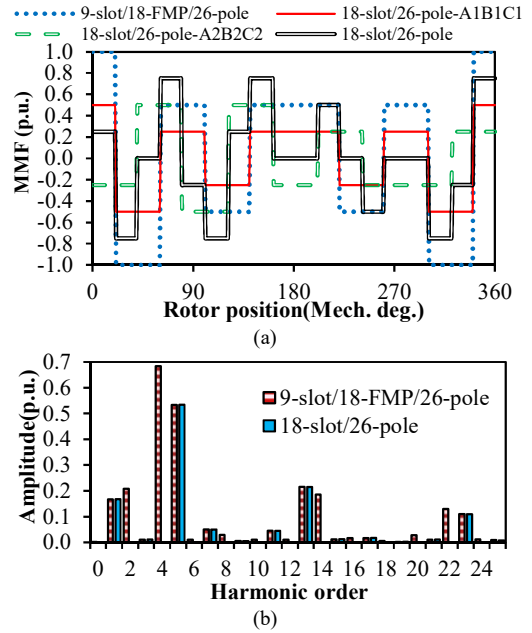


Fig. 3. MMF waveforms and spectra. (a) Waveforms (b) Spectra

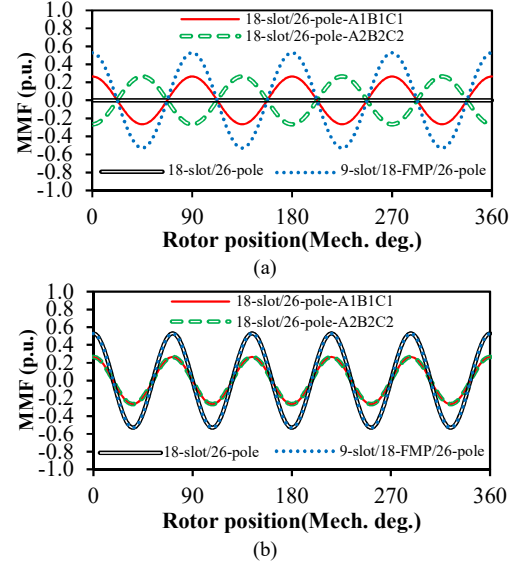


Fig. 4. Harmonic reduction principle. (a) 4<sup>th</sup> harmonic (b) 5<sup>th</sup> harmonic

### III. GLOBAL OPTIMIZATION AND PERFORMANCE COMPARISON

In this section, both of the 9-slot/18-FMP/26-pole and 18-slot/26-pole VPMSMs will be globally optimized and their performance will be compared.

#### A. Global Optimization

To make a fair comparison, both VPMSMs have been globally optimized to achieve the maximum torque under the following constrains: (1) Fixed stator outer radius  $r_o$ ; (2) Fixed air-gap length  $l_a$ ; (3) Fixed stack length  $l_{ef}$ ; (4) Fixed shaft radius  $r_s$ ; (5) Fixed copper loss at 75W considering the end windings for each machine; (6) Fixed slot packing factor; (7) Fixed overall PM volume. The related dimensional parameters are illustrated in Fig. 5. During the optimization, the stator yoke radius  $r_y$ , the stator inner radius  $r_i$ , slot opening angle  $a_{so}$ , stator teeth width  $w_t$ , PM length  $l_{pm}$  and the slot opening height  $h_{so}$  are variables for both machines. The FMP width  $w_f$  and height  $h_f$  are variables only for the 9-slot/18-FMP/26-pole VPMSM. The optimization is carried out by genetic algorithm. The optimized results are shown in Table I, where  $N_t$  stands for the number of turns per phase. It can be seen that the 18-slot/26-pole machine has more turns per phase than the 9-slot/18-FMP/26-pole machine as a result of larger optimized slot area and the same slot filling factor.

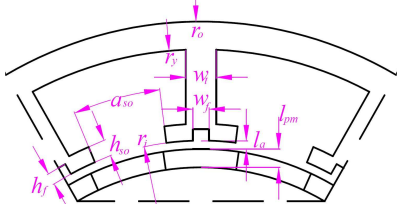


Fig. 5. Dimensional parameters in the optimization.

TABLE I  
OPTIMIZED PARAMETERS

|                       | 9-slot/18-FMP/26-pole | 18-slot/26-pole |
|-----------------------|-----------------------|-----------------|
| $r_o$ (mm)            | 50                    |                 |
| $l_a$ (mm)            | 1                     |                 |
| $r_s$ (mm)            | 5                     |                 |
| $l_{ef}$ (mm)         | 50                    |                 |
| $r_y$ (mm)            | 47.3                  | 48.2            |
| $r_i$ (mm)            | 32.7                  | 36.0            |
| $w_t$ (mm)            | 5.4                   | 2.9             |
| $h_{so}$ (mm)         | 5.1                   | 1.5             |
| $a_{so}$ (mech. deg.) | 5.6                   | 4.5             |
| $l_{pm}$ (mm)         | 3.3                   | 3.0             |
| $N_t$                 | 102                   | 126             |
| $h_f$ (mm)            | 2                     | -               |
| $w_f$ (mm)            | 10.2                  | -               |

#### B. No-load Performance Comparison

The phase back EMF waveforms and spectra for both machines are calculated by finite element analysis (FEA) and shown in Fig. 6. The phase back EMF fundamental harmonic of the 18-slot/26-pole machine is 18.7% larger than the 9-slot/18-FMP/26-pole machine as a result of larger number of turns per phase. It also shows that the 18-slot/26-pole machine has a larger 3<sup>rd</sup> harmonic component whereas it can be eliminated in the line waveforms.

#### C. Torque Performance Comparison

Fig. 7 and Table II compare the torque waveforms when the end windings are considered and the copper loss for both

machines are fixed at 75W. It shows the 18-slot/26-pole machine has almost the same average torque with the 9-slot/18-FMP/26-pole machine. However, both the peak to peak torque and torque ripple index (the ratio of peak to peak torque to average torque) of the 18-slot/26-pole machine are smaller. The torque with respect to different copper loss is shown in Fig.7 (b), it shows that at smaller copper loss, both machines have similar torque output whereas the 18-slot/26-pole machine has larger torque output when the copper loss increases. This is because the 18-slot/26-pole machine has better overload capability as a result of the reduced armature reaction MMF harmonics.

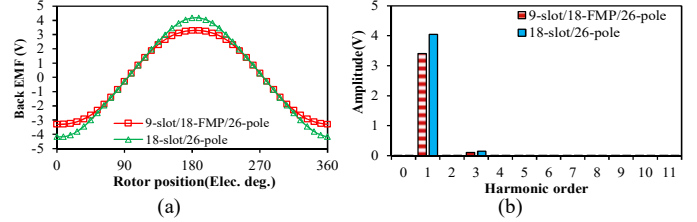


Fig. 6. Back EMF comparison (100rpm). (a) Waveform (b) Spectrum

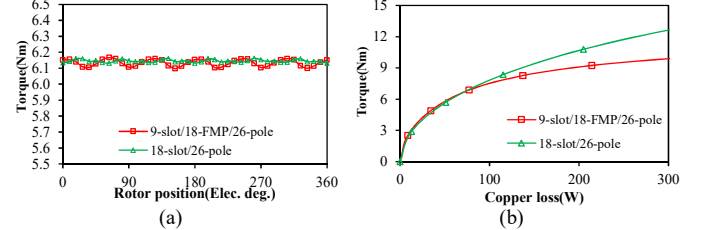


Fig. 7. Torque comparison. (a) Torque waveforms at copper loss of 75W (b) Torque vs copper loss

#### D. Inductance and Power Factor Comparison

To make a fair comparison, both q-axis inductance and inductance per turn of both machines are calculated and compared in Table II. It shows that the 18-slot/26-pole machine has both smaller  $L_q$  and  $L_q/N_t$ . It is noteworthy that the FEA calculated  $L_q/N_t$  of the 18-slot/26-pole machine is 42% of the 9-slot/18-FMP/26-pole machine, which is consistent with the analytical results calculated by (3). Despite the fact that the 18-slot/26-pole machine has larger  $N_t$ , it has smaller  $L_q$  as a result of even smaller  $L_q/N_t$ . Under the same working condition, the fundamental harmonics of the induced voltage of both machines are shown in Fig. 8. It shows clearly that the power factor angle  $\varphi_2$  is smaller than  $\varphi_1$ . From (1) it can be calculated that the 18-slot/26-pole machine improves the power factor from 0.73 to 0.95 as shown in Table II.

TABLE II  
PERFORMANCE COMPARISON

|                          | 9-slot/18-FMP/26-pole | 18-slot/26-pole |
|--------------------------|-----------------------|-----------------|
| Torque (Nm)              | 6.13                  | 6.14            |
| Peak to peak torque (Nm) | 0.07                  | 0.03            |
| Torque ripple (%)        | 1.12                  | 0.49            |
| $L_q$ (mH)               | 2.72                  | 1.24            |
| $L_q/N_t$ (mH)           | 0.026                 | 0.011           |
| $\cos\varphi$            | 0.73                  | 0.95            |
| $k_{wf}$                 | 3.04                  | 1.31            |

#### E. Flux Weakening Capability Comparison

The flux weakening capabilities of the two machines are calculated when the maximum DC voltage and phase current  $I_{max}$  of the inverter are set to be 100V and 30A, respectively.

Fig. 9 shows the torque-speed and power-speed curves for both machines. It shows that the 18-slot/26-pole machine has 50% larger torque and 18% larger base speed as a result of larger torque at larger excitation and smaller inductance, respectively. As a result, the 18-slot/26-pole machine has a larger constant power in the flux weakening region. The flux weakening factor, defined as  $k_{wf} = L_d I_{max} / \psi_d$ , where  $L_d$  is the d-axis inductance and  $\psi_d$  is the d-axis flux linkage, is also calculated and compared in Table II. It shows that  $k_{wf}$  of the 18-slot/26-pole machine is closer to 1, resulting in higher power capability at high speed.

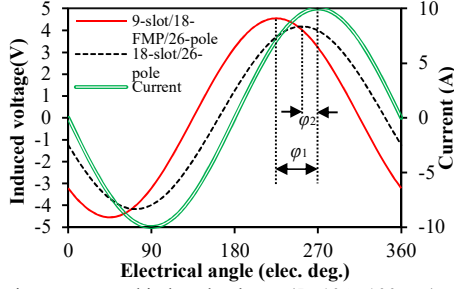


Fig. 8. Injecting current and induced voltage. ( $I_a=10A$ , 100rpm)

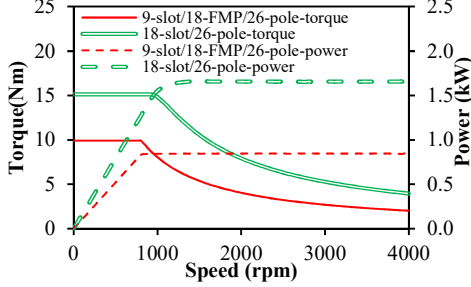


Fig. 9. Torque and power vs speed.

#### IV. DESIGN PRINCIPLE AND GUIDELINES

For a  $N_s$ -slot/ $N_f$ -FMP/ $2p_r$ -pole VPMSM with concentrated windings, as long as it satisfies  $1/2N_fN_s=2(N_f-p_r)\pm 1$ , the main armature reaction MMF harmonics will appear in pairs with the order difference of 1 [14][15]. Hence, the armature reaction MMF harmonics of even (or odd) orders can be eliminated by doubling the slot numbers and configuring the windings in the way shown in Table III. Since  $N_f$  is an even number, if  $N_f-p_r$  is even,  $p_r$  is also even and the odd harmonics can be eliminated by adopting steps (1)-(4) described in Section II B. If  $N_f-p_r$  is odd, the even harmonics can be eliminated by adopting steps (1)-(5) described in Section II B. By doing this, the space harmonic content as well as the inductance will be reduced, and hence, the power factor will increase. Typical slot/pole combinations and their relationships are also provided in Table III.

TABLE III  
WINDING CONFIGURATION METHOD

| concentrated tooth coil windings<br>$N_s$ -slot/ $N_f$ -FMP/ $2p_r$ -pole | $\Rightarrow$ |         | coil pitch=2 slot pitches<br>$N_f$ -slot/ $2p_r$ -pole |
|---|---------------|---------|--|
| $1/2N_fN_s=2(N_f-p_r)\pm 1$   | $N_f-p_r$     | Steps   | $N_s=N_f(4p_r\pm 2)/3$                                 |
| 9-slot/18-FMP/28-pole   | Even          | (1)-(4) | 18-slot/28-pole  |
| 9-slot/18-FMP/26-pole   | Odd           | (1)-(5) | 18-slot/26-pole  |

#### V. EXPERIMENTAL VALIDATION

To validate the previous analyses, the 18-slot/26-pole

VPMSM is prototyped. Figs. 10 (a) and (b) show the photos of stator and rotor. The dimensional parameters are provided in Table I. Firstly, the back-EMF is tested and compared with the FEA result, Fig. 11 (a). The static torque waveforms within 0–180 electric degrees and under different currents are also tested and compared with the FEA results. The test is done by applying DC current to the windings ( $I_b=I_c=-I_a/2$ ) and obtaining the static torque from the test rig shown in Fig. 10 (c) [14]. The q-axis inductance is also tested by a LCR meter [15] and the power factor is calculated by (1) and shown in Table IV. Although there are some discrepancies between the FEA and measured results due to the end effect and manufacturing tolerance, good agreements are obtained.

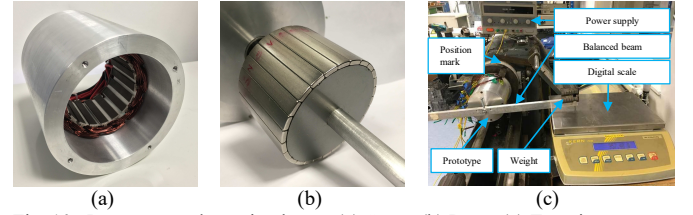


Fig. 10. Prototype and test rig photos. (a) Stator (b) Rotor (c) Test rig

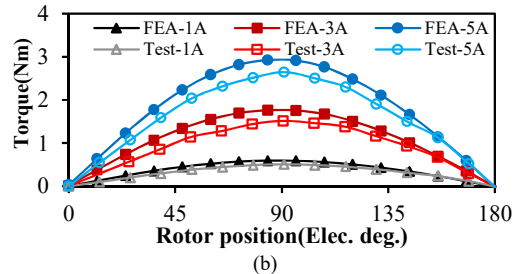
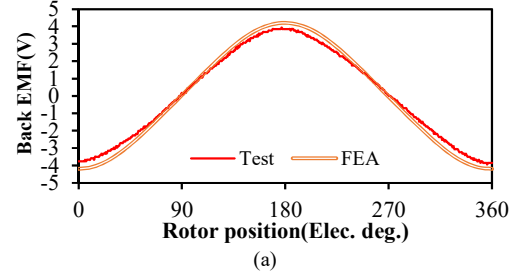


Fig. 11. Comparison of the measured and FEA predicted results. (a) Back EMF(100rpm) (b) Static torque

TABLE IV  
INDUCTANCE MEASUREMENT AND POWER FACTOR

|            | Measured | FEA predicted |
|------------|----------|---------------|
| $L_q$ (mH) | 1.25     | 1.39          |
| $\cos\phi$ | 0.92     | 0.95          |

#### VI. CONCLUSION

In this paper, an 18-slot/26-pole VPMSM with coil-pitch of two slot pitches is proposed from a 9-slot/18-FMP/26-pole VPMSM with concentrated windings. Compared with the original VPMSM, the proposed design reduces the armature reaction space harmonic content and phase inductance without affecting the fundamental harmonic, and hence increases the power factor with better torque and flux weakening capability. The study also shows that a series of VPMSMs with coil-pitch of two slot pitches can achieve high power factor based on the same design principle and given design guidelines. A prototype is manufactured and tested for validation.

## REFERENCES

- [1] L. Jian, G. Xu, C. C. Mi, K. T. Chau, and C. C. Chan, "Analytical method for magnetic field calculation in a low-speed permanent-magnet harmonic machine," *IEEE Trans. Energy Convers.*, vol. 26, no. 3, pp. 862–870, Sep. 2011.
- [2] D. Li, R. Qu, and J. Li, "Analysis of torque capability and quality in Vernier permanent-magnet machines," *IEEE Trans. Ind. Appl.*, vol. 52, no. 1, pp. 125–135, Jan./Feb. 2016.
- [3] W. N. Fu and S. L. Ho, "A quantitative comparative analysis of a novel flux-modulated permanent-magnet motor for low-speed drive," *IEEE Trans. Magn.*, vol. 46, no. 1, pp. 127–134, Jan. 2010.
- [4] J. Yang, G. Liu, W. Zhao, Q. Chen, Y. Jiang, L. Sun, and X. Zhu, "Quantitative comparison for fractional-slot concentrated-winding configurations of permanent-magnet Vernier machines," *IEEE Trans. Magn.*, vol. 49, no. 7, pp. 3826–3829, July 2013.
- [5] J. Li, K. T. Chau, and W. Li, "Harmonic analysis and comparison of permanent magnet vernier and magnetic-geared machines," *IEEE Trans. Magn.*, vol. 47, no. 10, pp. 3649–3652, Oct. 2011.
- [6] B. Kim and T. A. Lipo, "Operation and design principles of a PM Vernier motor," *IEEE Trans. Ind. Appl.*, vol. 50, no. 6, pp. 3656–3663, Nov./Dec. 2014.
- [7] Y. Kataoka, M. Takayama, Y. Matsushima, and Y. Anazawa, "Comparison of three magnet array-type rotors in surface permanent magnet-type vernier motor," in *Proc. Int. Conf. Elect. Mach. Syst.*, pp. 1–6, Oct. 2012.
- [8] D. Li, R. Qu, and T. A. Lipo, "High-power-factor Vernier permanent-magnet machines," *IEEE Trans. Ind. Appl.*, vol. 50, no. 6, pp. 3664–3674, Nov./Dec. 2014.
- [9] F. Zhao, T. A. Lipo, and B. Kwon, "A novel dual-stator axial-flux spoke-type permanent magnet vernier machine for direct-drive applications," *IEEE Trans. Magn.*, vol. 50, no. 11, pp. 2–5, Nov. 2014.
- [10] Y. Liu and Z. Q. Zhu, "Electromagnetic performance comparison of 18-slot/26-pole and 18-slot/10-pole fractional slot permanent magnet surface-mounted machines," *20th Int. Conf. Electr. Mach. Syst.*, Aug. 2017.
- [11] D. Li, T. Zou, R. Qu, and D. Jiang, "Analysis of fractional-slot concentrated winding PM Vernier machines with regular open-slot stators," *IEEE Trans. Ind. Appl.*, vol. 54, no. 2, pp. 1320–1330, March./April 2018.
- [12] K. Okada, N. Niguchi, and K. Hirata, "Analysis of a Vernier motor with concentrated windings," *IEEE Trans. Magn.*, vol. 49, no. 5, pp. 2241–2244, May 2013.
- [13] A. M. EL-Refaie and T. M. Jahns, "Optimal flux weakening in surface pm machines using fractional-slot concentrated windings," *IEEE Trans. Ind. Appl.*, vol. 41, no. 3, pp. 790–800, May/June 2005.
- [14] J. Wang, V. I. Patel, and W. Wang, "Fractional-slot permanent magnet brushless machines with low space harmonic contents," *IEEE Trans. Magn.*, vol. 50, no. 1, pp. 1–9, Jan. 2014.
- [15] K. Wang, Z. Q. Zhu, and G. Ombach, "Synthesis of high performance fractional-slot permanent-magnet machines with coil-pitch of two slot-pitches," *IEEE Trans. Energy Convers.*, vol. 29, no. 3, pp. 758–770, Sep. 2014.
- [16] Z. Q. Zhu, "A simple method for measuring cogging torque in permanent magnet machines," *IEEE Power Energy Soc. Gen. Meet.*, pp. 3–6, Oct. 2009.
- [17] Y. Liu, Y. Pei, Y. Yu, Y. Shi, and F. Chai, "Increasing the saliency ratio of fractional slot concentrated winding interior permanent magnet synchronous motors," *IET Electr. Power Appl.*, vol. 9, no. 7, pp. 439–448, Jul. 2015.